Isolation and characterization of fucosylated extracellular vesicles based on a novel GlyExo-Capture technique

Boan Li[#a], Kun Hao[#b,d], Zhengtai Li[c], Cuidie Ma[c], Hongjiang Li[c], Wenqian Du[b], Lijuan Sun[b], Tianye jia[a], Aixia Liu[a], Yanzhao Li[b], Lida Xu*[c], Qi Gao*[b,e], Ruifu Yang*[d,e], Changqing Lin*[b]

[a]Department of Laboratory Medicine, Fifth Medical Center of PLA General Hospital, Beijing 100039, P.R. China

[b]Beijing Glyexo Gene Technology Co., Ltd., Beijing 102600， P.R. China

[c]College of Life Science and Technology, Beijing University of Chemical Technology, Beijing, 100029, P.R. China

[d]State Key Laboratory of Pathogen and Biosecurity, Beijing Institute of Microbiology and Epidemiology, Beijing 100071, P.R. China

[e]Beijing Key Laboratory of POCT for Bioemergency and Clinic (No. BZ0329), Beijing 100071, P. R. China

[#]These authors contributed equally to the work.

*Correspondence: xuld@mail.buct.edu.cn(L.X.), qi.gao@hotgen.com.cn(Q.G.), ruifuyang@gmail.com(R.Y.), changqinglin2021@163.com(C.L.)

ABSTRACT

Extracellular vesicles (EVs) derived from tumor cells have recently garnered great interest due to their diagnostic and therapeutic potential. The presence of different glycosylation at the EVs surface potentiates the need for efficient glycosylated-EVs isolation. Here, we developed a GlyExo-Capture technique for capturing fucosylated-EVs from serum and cell supernatants robustly. Lens culinaris lectin (LCA)-immobilized beads were found to capture approximately 60% of the total EVs from HepG2 cells. The capture efficiency was reduced to lower than 40% in non-tumorigenic MIHA cells. Notably, the cellular uptake pattern of highly fucosylated-EVs was markedly different from EVs with low fucosylation. The disclosure of enriched fucosylated-EVs miRNA cargos by next-generation deep sequencing revealed 75 differentially expressed miRNAs in hepatocellular carcinoma (HCC). Among them, a 4-miRNA panel was chosen and yielded an area under the ROC curve (AUC) of 0.86 and 0.84 for the detection of HCC from non-HCC controls in testing sample and an independent validation sample, respectively. The 4-miRNA signature was independent of AFP and a combined model with AFP yielded an increased AUC of 0.92. In conclusion, we developed a high-throughput method for capturing fucosylated-EVs efficiently and shed light on using fucosylated-EVs as potential sources of miRNA for cancer biomarker detection.

KEYWORDS: GlyExo-Capture technique; fucosylated-EVs; miRNA; lectin; hepatocellular carcinoma.

Introduction

Extracellular vesicles (EVs) are small, nanosized particles with lipid bilayer membranes that carry proteins, DNA, RNA, and metabolites [1]. EVs play diverse roles in intercellular communication, normal physiological processes, and tumor development [2-4]. EVs exist prevalently in human bodily fluids and can be secreted by various types of cells [5]. Compared with non-tumor cells, tumor cells have different amounts and compositions of EVs [6,7]. Tumor cells always have a 'sweeter' surface, and tumor-associated glycan alterations have already been identified as enriched in cancer EVs [8,9]. These glycan-coated EVs can be described as 'sugar-coated bullets' fired by tumor cells [10]. The presence of different glycosylation profiles under normal and cancer conditions highlights the importance of studying glycosylated-EVs and their specific miRNA cargos in cancer diagnosis and therapy [8,11-13].

Traditional EVs isolation methods, including ultracentrifugation, microfiltration, and size exclusion chromatography, are based on EVs size and buoyant density [14,15]. Recent immune affinity or microfluidic technologies are based on the exposed components on the EVs surface. Glycans constitute a valuable source of targets to capture and isolate EVs from a heterogeneous sample due to their abundance on the EVs surface. For example, lectins peanut agglutinin (PNA), *Artocarpus integrifolia* (AIA or Jacalin), or *Maackia amurensis* lectin I (MAL-I) are used to isolate EVs of different sizes from human urinary samples based on their high affinity for Gal or GalNAc residues with a (2,3)-linked sialic acid [8]. A similar

approach is applied to isolate EVs from urine samples by *Solanum tuberosum* lectin (STL) lectin based on its interaction with N-acetylglucosamine and lactosamine residues [8]. A nanoparticle-based time-resolved fluorescence immunoassay (NP-TRFIA) captures EVs from urine samples and cell supernatants based on the tetraspanins and glycan antigens present at the EVs surface [16]. Apart from affinity-based isolation methods, a commercially available precipitation kit called ExoGAG precipitates EVs out of the solution due to the presence of negatively charged GAG at the EVs surface [17]. Despite the technological advances in this field, less laborious isolation methods are still technically challenging.

In this study, we developed a GlyExo-Capture technique aiming to capture EVs by using fucose-specific lens culinaris lectin (LCA) for affinity isolation. This GlyExo-Capture technology enriched fucosylated-EVs from serum samples and cell supernatants over a short period and with high throughput. The characterization of enriched fucosylated-EVs and the diagnostic value of fucosylated-EVs specific miRNA was also demonstrated, with the potential to be translated into the clinical setting.

Material and Methods

Patient enrolment and study cohorts

The study was approved by the Ethics Committee of the Fifth Medical Center of Chinese PLA General Hospital (2016-004-D). Patients included in the study were >18 years of age. Exclusion criteria were pregnancy, immunosuppression, leukopenia, haematological malignancies or the initiation of palliative care. All patients with HCC were treatment-naïve at the time of blood sampling. Three independent cohorts were included:

1. Disclosure of miRNA profiles derived from fucosylated-EVs by NGS was conducted in a cohort including 61 HCC patients, 24 hepatitis patients and 30 healthy subjects. Healthy subjects and hepatitis patients were included as the non-HCC group. This cohort referred as original sample was randomly divided into a training sample and a testing sample at a ratio of about 7:3. The training sample was used for constructing prediction models based on the 4-miRNA signature in fucosylated-EVs, while the testing sample was used to measure the predict efficiencies of models.

2. An independent cohort including 16 HCC patients, 16 hepatitis patients and 16 healthy subjects was included in this study to confirm NGS data by RT-qPCR.

3. An independent cohort including 52 HCC patients, 30 hepatitis patients and 23 healthy subjects was included as validation sample to evaluate the 4-miRNA-based diagnostic potential.

Sample collection

Blood was drawn by venipuncture using 21-gauge needle. In order to prevent haemolysis, aspiration was performed slowly and evenly for both procedures. Blood was collected in 5 ml vacuum tubes containing separator gel (Improve Medical Instruments Co., Ltd, Guangzhou, China) and centrifuged at 1800 g for 10 min at room temperature (RT) within 1 hour of sampling. Resulting serum was centrifuged again at 3000 g for 10 min at 4 ℃to remove cellular debris. Then the serum was aliquoted and stored at −80 ℃.

Reagents and resources

The key reagents and resources used in this research were listed in Supplemental Table 1.

Cell culture and EVs purification

HepG2 (CRL-10741), HCT-116 (CCL-247), and Hela (CCL-2) cell lines were obtained from the American Type Culture Collection (ATCC, Rockville, USA). MIHA (CE18544) cell line was obtained from Beijing Crisprbio Biotechnology Co., Ltd. All cell lines were tested for mycoplasma contamination and were expanded in DMEM supplemented with 10% (v/v) fetal bovine serum (FBS; GIBCO, Life Technologies, Carlsbad, USA), 0.1 mg/mL streptomycin, 0.25 μg/mL amphotericin B and 100 units/ml penicillin (Sangon Biotech Co., Ltd., Shanghai, China), at 37 °C with 5% of CO_2. For EVs production, HepG2 cells were maintained in EVs-depleted media and the conditioned media was collected after 72 hours and centrifuged at 300 g for 10 min to remove cells.

Serum or cell supernatant were diluted 1:2 with cold PBS before low-centrifugation at 3000 g for 10 min to remove cellular debris. The resulting supernatant was then transferred to new tubes and divided into two parts. One part was ultracentrifuged at 100,000 g using a type 100 TI rotor of XPN-100 (CP100NX; Hitachi, Brea, USA) for 90 min and the resulting EVs pellet was resuspended in 250 ml of cold PBS and was denoted as UC-EVs. One part was incubated with LCA-immobilized beads and the bound fraction was denoted as highly fucosylated-EVs (HF-EVs). The unbound fraction was subjected to ultracentrifuge at 100,000 g for 90 min and the resulting EVs pellet was denoted as low fucosylated-EVs (LF-EVs). To test the specificity of GlyExo-Capture kit, 20 μg EVs were treated with 2 μL PNGase F (882U/μL, Yeasen Biotechnology Co. Ltd., Shanghai, China) for 12 hours before the cellular uptake assay. The protein content of EVs was quantified using Qubit Protein Assay (Invitrogen, Pittsburg, USA) and a Qubit3.0 fluorometer (Invitrogen, Pittsburg, USA).

Transmission electron microscopy (TEM)

EVs isolated by ultracentrifuge or GlyExo-Capture were fixed with 2% glutaraldehyde for 1 hour at RT and stained with 0.5% uranyl acetate (pH 4.5). TEM was performed on a FEI Tecnai Spirit ((FEI, Eindhoven, NL) at 120 kV. Electron micrographs were captured with a Gatan UltraScan 1,000 CCD camera (Gatan, Pleasanton, USA).

Nanoparticle tracking analysis (NTA)

EVs isolated by ultracentrifuge or GlyExo-Capture were analyzed for particle concentration and size distribution using the Malvern NanoSight NS300 (Malvern Instruments Ltd., Malvern, UK) in accordance with the manufacturer's instructions.

Briefly, three independent replicates of diluted EVs preparations in PBS were injected at a constant rate into the tracking chamber using the provided syringe pump. The specimens were tracked at RT for 60 s. Shutter and gain were adjusted and were kept at optimized settings for all samples manually. The data were captured and analyzed with NTA Build 127 software version 2.3.

Western blot analysis

EVs isolated by ultracentrifuge or GlyExo-Capture were lysed and protein concentration was analyzed using Qubit Protein Assay (Invitrogen, Pittsburg, USA) and a Qubit3.0 fluorometer (Invitrogen, Pittsburg, USA). Input for EVs was normalized to 25 μg total protein. Proteins were separated by SDS–PAGE and transferred to 0.45 μm nitrocellulose membrane (GE Healthcare Life Sciences, Marlborough, USA). Membranes were blocked with 1% non-fat milk powder and incubated with primary antibodies. The secondary antibodies were rabbit anti-mouse IgG-HRP and protein bands were detected using the BeyoECL Plus Detection System (Beyotime Biotechnology, Shanghai, China). Primary antibodies used were anti-CD81 (M38) (1:400 dilution, Abcam, Cambridge, USA), anti-Alix (3A9) (1:400 dilution, Abcam, Cambridge, USA), anti-TSG101 (4A10) (1:400 dilution, Abcam, USA) and anti-calnexin (EPR3633(2)) (1:2000 dilution, Abcam, Cambridge, USA).

Exoview analysis

EVs isolated by ultracentrifuge or GlyExo-Capture were added to chips printed with antibodies including anti-human CD81 (JS-81), anti-human CD63 (H5C6), anti-human CD9 (HI9a), and anti-mouse IgG1 (MOPC-21) antibodies on ExoView R100 (NanoView

Biosciences, Brighton, USA). All chips were imaged in an ExoView scanner (NanoView Biosciences, Brighton, USA) and data were analyzed using NanoViewer 2.8.10 Software (NanoView Biosciences, Brighton, USA).

Cellular uptake assay using flow cytometry

Cellular uptake of HF-EVs, HF-EVs treated with PNGase F, LF-EVs, and LF-EVs treated with PNGase F were studied using flow cytometry. Briefly, the cells were exposed to DiD-labeled EVs at the indicated doses and then incubated at 37 °C for the indicated time points. After extensive wash, flow cytometry was performed with a BD FACSCanto II instrument (BD Biosciences, San Jose, USA) and 45 second acquisitions under a medium flow rate were used for data capture. Data analysis was performed using FlowJo software with gating of cells in the PE channel and no impact was found for equivalent DiD background samples. A control sample of DiD dye background was prepared following the same procedures as indicated above but without using any cells.

RNA isolation and analysis

Total RNA from EVs was extracted using a miRNeasy® Mini kit (cat. 217,004, Qiagen, Hilden, German) according to standard protocol and was assessed using the High Sensitivity RNA Cartridge of the Qsep100 fully automatic nucleic acid analysis system (Bioptic Inc., LA, USA).

Next-Generation Sequencing and bioinformatics analysis

EVs-RNA was converted into cDNA libraries using the NEBNext1 Small RNA Library Prep Set for Illumina1 (Multiplex Compatible) (Cat No.: E7330, NEB, Ipswich, USA)

following the manufacturer's instructions. Library size was selected using the E-Gel SizeSelect II gel of the E-Gel Power Snap electrophoresis system (Thermo Fisher Scientific Inc., Waltham, USA). Pooled libraries with unique barcodes were loaded on 318 sequencing chips and run on the Ion Torrent Personal Genome Machine (Life Technologies, Carlsbad, USA). The Torrent Suite 3.4.1 was used to manage the Ion Torrent PGM to process raw signals and perform base calling. The sequences were then assessed for quality and primer-adapter sequences were trimmed by the Cutadapt software, followed by alignment to the human reference genome (HG38) by Bowtie. The aligned data was annotated by the HT-seq with the gff3 file from miRBase V23. The number of reads for each miRNA was normalized to transcript per million (TPM) across all samples. Data have been uploaded to SRA database with the BioProject number PRJNA785786.

The miRNA count data were normalized, and differential analysis was conducted using the DESeq2 package in R 4.1.0. All tests were two-tailed, and the false discovery rate (FDR) was used for multiple comparisons. Fold changes larger than 2 and adjusted p-value less than 0.05 were used to select differentially expressed miRNAs in the volcano plot. Heatmap (v1.0.12) was used for clustering with the Euclidean distance method. Linear discriminant analysis of the TPM expression matrix was conducted using the MASS package (v7.3) to visualize the separation of HCC and non-HCC. Target genes of DEMs were predicted using miRPath on the DIANA website (http://snf-515788.vm.okeanos.grnet.gr/).

Real-time quantitative PCR (RT–qPCR)

cDNA was synthesized using a miRcute plus miRNA cDNA first strand synthesis kit (cat. No. KR211) according to a standard protocol (Tiangen Biotech Co. Ltd., Beijing, China). RT–qPCR was performed by a miRcute plus miRNA qPCR kit (SYBR Green) (Tiangen Biltech Co. Ltd., Beijing, China) on an ABI 7500 real-time PCR system (Applied Biosystems, Foster City, USA). The relative levels of individual miRNAs were calculated after normalization to the miR16 and let7a level in the corresponding sample. The specific primers used for RT–qPCR are synthesized by Sangon biotech (Shanghai) Co. Ltd. and listed in Supplemental Table 2.

Multivariate analysis to select miRNA markers

Adaboost model and support vector machine (SVM) model were utilized to complementarily evaluate the value of miRNAs in discriminating the HCC and non-HCC groups. Based on the AdaBoost algorithm with the R package "adabag", the importance of miRNA i is defined as its weighted frequency presented in the model containing 100 weighted trees (cross-validation = 10). We sampled 75% of the original samples randomly for 30 times, to get the miRNAs' average importance scores. Meanwhile based on the linear SVM model, the importance of gene i could be measured as

$$Imp(i) = \frac{|\alpha_i|}{||W||^2}$$

in which $W = \{\alpha_i\}$ was the coefficient vector perpendicular to the support vectors. Then the miRNAs' average importance scores were derived by sampling 75% of the original samples randomly for 500 times.

With the two definitions of importance above, the miRNA with the minimum importance score was deleted one by one from the DEM combination. The false discovery rate (FDR), defined as the ratio of the prediction error rate on the original data to that on label permutated data, was used to evaluate the miRNA combinations' predictive effect and determine the optimal miRNA panel.

Prediction Modeling

The Z-score original data was randomly divided into a training set and a testing set at a ratio of 7:3. We compared the performances and stabilities of nine common models in the sklearn package by bootstrap sampling the training set 100 times. Then the prediction capabilities of two models with higher AUC values and lower standard deviations were evaluated on the testing set. Furthermore, the signature panel was validated in a subsequent study.

SVC models were constructed with the combination of AFP and miRNA signature panel and with either AFP or miRNA signature panel, respectively. To compare their performance, we fit the mean of ROC curves and calculated the 95% confidence interval using the “roc-utils” package with 100 times bootstrap samplings.

Statistical analysis

The present study used GraphPad Prism 8.0 (GraphPad Software Inc., San Diego, USA) for statistical calculations and data plotting. Differences between two independent samples in figure 2 and figure 3 were evaluated using two-tailed Student’s t-tests. Since the expression of miRNA was not followed normal distribution according to the Shapiro-Wilk test, differently expressed miRNA were evaluated using the

Mann-Whitney test in figure 4, figure 5, and figure 6. All tests were two-tailed unless otherwise indicated. We considered a P value ≤ 0.05 to be statistically significant. Significance values were set as follows: ns (not significant), P > 0.05; *, P < 0.05; **, P < 0.01; and ***, P < 0.001.

Results

Fucosylated-EVs enrichment based on the GlyExo-Capture method

To capture fucosylated-EVs, a GlyExo-Capture method was developed by immobilizing LCA on hydroxyl magnetic beads. The reagents were prepackaged in advance in a 96-well plate, and the whole isolation process took approximately 11 minutes. The workflow of the GlyExo-Capture method was summarized in Figure 1, and detailed information is listed in Supplemental Table 3. EVs isolated by the differential ultracentrifugation method (UC-EVs) were used as controls. TEM analysis showed that the fucosylated-EVs and UC-EVs were oval- or bowl-shaped (Figure 2(a,b)). The average size of fucosylated-EVs (106.5±6.7 nm) was smaller than the average size of UC-EVs (137.5±0.4 nm), but fucosylated-EVs had a broader size distribution (Figure 2(a,b)). Immunoblot and ExoView analysis showed the expression of tetraspanins, TSG101, and ALIX (Figure 2(c,d)), indicating the successful isolation of fucosylated-EVs from the serum samples. Of note, increased staining intensity of tetraspanins was observed in fucosylated-EVs compared to UC-EVs when the same doses of EVs were used, indicating that higher EVs purification was achieved using this GlyExo-Capture method (Supplemental Figure 1).

To estimate the binding efficiency of LCA-immobilized beads, the UC-EVs were incubated with LCA-immobilized beads or BSA-immobilized beads, and the unbound fractions were subjected to quantitative analysis. The analysis showed that incubation of UC-EVs with LCA-immobilized beads, but not BSA-immobilized beads, resulted in a significant decrease in UC-EVs particle numbers in the unbound fraction by 40%, indicating that approximately 60% of HepG2-derived EVs were captured by LCA-immobilized beads (Figure 2(e)). Specifically, the proportion of fucosylated-EVs secreted by MIHA, non-tumorigenic hepatocyte cell line, was lower than 40% (Figure 2(f)). Therefore, GlyExo-Capture is a fast and reliable method to isolate fucosylated-EVs from the cell supernatant and human serum in a high-throughput manner.

Cellular uptake of fucosylated-EVs

To characterize the fucosylated-EVs, the uptake patterns of the fucosylated-EVs by their parent cells were first evaluated. To this end, the EVs collected by GlyExo-Capture beads were identified as enriched or highly fucosylated-EVs (HF-EVs), and the unbound supernatant subjected to differential ultracentrifugation was identified as low fucosylated-EVs (LF-EVs). These EVs were labeled with the fluorescent dye DiD, and the uptake behaviors were analyzed by flow cytometry. As was shown, HF-EVs showed time- and dose- dependent uptake manner (Figure 3(a,b)). Notably, HF-EVs exhibited significantly higher uptake efficiency than EVs with low fucosylation (Figure 3(c,d)). Of note, the enzymatic removal of N-glycans through PNGase F reduced the enhanced uptake efficiency of HF-EVs to levels comparable to

LF-EVs (Figure 3(c,d)). Thus, the glycosylated form of EVs may be responsible for their adherence and internalization.

After demonstrating the improved uptake of HF-EVs by their parent cells, we further evaluated whether this phenomenon was cell specific. To this end, LF-EVs and HF-EVs labeled with DiD and released from HepG2 cells were exposed to diverse cells. In consistent with the above result, HepG2 HF-EVs were also quickly loaded by HCT-116 and Hela cells (Figure 3(e,f)), which indicates a specific targeting behavior of fucosylated-EVs.

miRNA profiles of fucosylated-EVs in hepatocellular carcinoma (HCC)

As glycans are highly expressed on cancer EVs, the disclosure of enriched fucosylated-EVs miRNA cargos may hold a tremendous potential to identify more specific and sensitive cancer EVs biomarkers. To this end, a cohort of 61 HCC patients, 24 hepatitis patients and 30 healthy subjects were recruited. Next-generation deep sequencing (NGS) was used to identify the global profile of the fucosylated-EVs miRNA cargo. For each sample, at least 15 M raw reads were generated, and a total of 1,938 known miRNAs were identified. Hepatitis and healthy subjects were combined as non-HCC controls unless otherwise referred. In the differentially expressed miRNA (DEM) analysis (Fold changes>2, $p<0.05$), 52 miRNAs were upregulated and 23 were downregulated in the HCC group compared with the non-HCC group (Supplemental Figure 2; Supplemental Table 4). Linear discriminant analysis (LDA) based on the expression matrix of 75 DEMs showed that three distinct clusters were generally classified as HCC, hepatitis, and healthy groups (Figure 4(a)).

Compared with DEMs in The Cancer Genome Atlas (TCGA) dataset, 19 DEMs of the fucosylated-EVs showed the same expression profiles (Figure 4(b)). Of note, the targeted mRNAs were mainly enriched in pathways in cancer, endocytosis, Ras signaling pathway, Rap1 signaling pathway, and proteoglycans in cancer (Supplemental Figure 3).

To verify the NGS data, another cohort of 48 participants (16 HCC, 16 hepatitis, and 16 healthy controls) was recruited, and 13 randomly selected DEMs were confirmed by RT–qPCR analysis. Except 1 DEMs, 12 out of 13 DEMs exhibited similar expression patterns as those detected with the NGS data (Figure 4(c,d)).

Identification of HCC-specific miRNA signatures in fucosylated-EVs

Using multivariate analysis, a panel of 6 miRNAs was selected from the 75 DEMs based on NGS results (Figure 5(a)). RT–qPCR results showed that miR-215-5p and miR-432-5p expression was either downregulated or unchanged in the HCC group (Figure 5(b)), whereas miR-483-5p, miR-182-3p, miR-651-5p, and miR-429 were all significantly upregulated in the HCC group (Figure 5(c)). The expression trend of these 4 miRNAs was consistent in RT-qPCR and NGS data (Figure 5(c)). Notably, these 4 miRNAs exhibited a low correlation with each other, which implied their high complementary feature in diagnosis use (Figure 5(d)). Therefore, the 4-miRNA panel from fucosylated-EVs was chosen as a signature for further biomarker analysis.

Diagnostic evaluation of the 4-miRNA signature in fucosylated-EVs

Based on the 4-miRNA signature in fucosylated-EVs, different prediction models including Gradient Boost, AdaBoost, Random Forest, Bagging, Decision Tree,

Gaussian NB, K Neighbors, SVC, and Logistic Regression were used. The cohort of 61 HCC patients, 24 hepatitis patients and 30 healthy controls were randomly divided into a training sample set and a testing sample set at a ratio of about 7:3. AdaBoost model and Random Forest model achieved higher AUC values with lower standard deviation (Figure 6(a)). Therefore, these two models were constructed to detect HCC samples. As was shown, the receiver operating characteristic curve (ROC) analysis of AdaBoost model showed that the 4-miRNA-based screening signature yielded an area under the ROC curve (AUC) of 0.86 for the detection of HCC from non-HCC controls in the testing sample (Figure 6(b)).

We next monitored to validate whether the 4-miRNA-based screening signature can discriminate HCC from non-HCC controls in another validation sample set comprised of 52 HCC patients, 30 hepatitis patients and 23 healthy controls. Specifically, we first evaluated the expression profiles of the 4-miRNA signature using RT-qPCR in the original samples and the validation samples. As expected, similar expression trends were observed in the two sample sets (Figure 6(c-f)). Of note, the 4-miRNA-based diagnostic signature also showed a great performance in predicting HCC (AUC: 0.84; Figure 6(g)). The 4-miRNA signature was independent of AFP (alpha-fetoprotein) and a combined model with AFP yielded an increased AUC of 0.92 (Figure 6(h)).

Discussion

Cancer EVs are rich in mannose, complex type N-glycans, polylactosamine, and sialylated glycans [11]. To date, several strategies have been developed to characterize the glycan profiles of EVs [8]. However, efficient and high-throughput isolation methods are still technically challenging. In this study, we developed a novel GlyExo-Capture technique to isolate EVs from serum samples and a panel of cancer cells using fucose-specific lens culinaris lectin. EVs captured by this GlyExo-Capture technique were morphologically intact with a broader size distribution pattern and increased purity compared to EVs isolated by ultracentrifugation, supporting the advantage of the immune affinity method over ultracentrifugation. The whole process of preparing 96 samples only took 11 minutes.

Reports have revealed the role and impact of glycosylation in EVs biodistribution and uptake [18]. It has been described that cleavage of terminal sialic acid residues accumulate more readily in the lungs and axillary lymph nodes than nontreated EVs [19]. For most of the cell lines tested, desialylated EVs had higher uptake efficiency [20]. Here, we found that the fucosylation of EVs strongly increased their uptake efficiency in parent cells and the other two cancer cell lines tested. Specifically, cleavage of EVs N-glycans by PNGase F digestion abolished the increase in the uptake of fucosylated-EVs. The different roles of sialic acid and fucose in the interaction between EVs and recipient cells need further investigation. Nevertheless, our results

interestingly suggest that EVs and cell fucosylation can impact EVs uptake, and therefore, may drive specific EVs organ biodistribution tropism.

One of the most critical aspects of glycosylated-EVs research is analyzing their nucleic acid cargo, particularly small RNAs [21]. Circulating miRNA biomarkers in the blood have been widely applied to disease diagnosis[22,23]. Previous studies indicated that miRNA biomarkers could be enriched in EVs [24-27]. The establishment of the GlyExo-Capture method makes the detection of serum fucosylated-EVs derived miRNA biomarkers a reality. We isolated fucosylated-EVs from serum samples of HCC and non HCC subjects by the GlyExo-Capture technique. Analysis of serum fucosylated-EVs derived miRNAs between the HCC and non-HCC groups showed the unique expression miRNA profile in the HCC group. Among the 75 DEMs from fucosylated-EVs, 19 DEMs were also identified in the HCC dataset from the TCGA, indicating that the miRNAs in the enriched fucosylated-EVs fractions could reflect the miRNA profile in the primary tumor site and may constitute critical miRNA functions in cancer progression. In particular, a panel of 4 miRNAs was chosen as a signature for HCC detection. Based on the samples in this study, the 4-miRNA panel shows great performance and significantly increases HCC detection efficiency in combination with AFP. The potential application of the GlyExo-Capture technique for pan-cancer detection warrants further investigation.

In summary, the GlyExo-Capture technique, which takes advantage of lectins in specifically selecting various types of glycans, can capture and enrich sugar-coated EVs efficiently and is user-friendly, fully automatic and robust. The high-throughput

feature potentiated the usage of this technique in tumor liquid biopsy and may open new avenues to delineate the roles of EVs glycosylation in cancer biology and therapy.

References

[1] Colombo M, Raposo G, Théry C. Biogenesis, secretion, and intercellular interactions of exosomes and other extracellular vesicles(J). Annual review of cell and developmental biology. 2014; 30: 255-289.

[2] Al-Nedawi K, Meehan B, Micallef J, et al. Intercellular transfer of the oncogenic receptor EGFRvIII by microvesicles derived from tumour cells. Nature Cell Biology. 2008; 10(5):619-24.

[3] Luga V, Zhang L, Viloria-Petit A, et al. Exosomes mediate stromal mobilization of autocrine Wnt-PCP signaling in breast cancer cell migration. Cell. 2012; 151(7):1542-1556.

[4] Chen L, Guo P, He Y, et al. HCC-derived exosomes elicit HCC progression and recurrence by epithelial-mesenchymal transition through MAPK/ERK signalling pathway. Cell Death & Disease. 2018; 9(5):513.

[5] Yang F, Liao X, Tian Y, et al. Exosome separation using microfluidic systems: size-based, immunoaffinity-based and dynamic methodologies. Biotechnology Journal. 2017; 12(4):1600699.

[6] An T, Qin S, Xu Y, et al. Exosomes serve as tumour markers for personalized diagnostics owing to their important role in cancer metastasis. Journal of extracellular vesicles. 2015; 4(1): 27522.

[7] Wang SE. Extracellular Vesicles and Metastasis. Cold Spring Harbor Perspectives in Medicine. 2019; 10(7):a037275.

[8] Martins ÁM, Ramos CC, Freitas D, et al. Glycosylation of cancer extracellular vesicles: capture strategies, functional roles and potential clinical applications. Cells. 2021; 10(1): 109.

[9] Bloise N, Okkeh M, Restivo E, et al. Targeting the "Sweet Side" of Tumor with Glycan-Binding Molecules Conjugated-Nanoparticles: Implications in Cancer Therapy and Diagnosis. Nanomaterials. 2021; 11(2):289.

[10] Lin S, Zhou S, Yuan T. The "sugar-coated bullets" of cancer: Tumor-derived exosome surface glycosylation from basic knowledge to applications. Clinical and Translational Medicine. 2020; 10(6):e204.

[11] Williams C, Royo F, Aizpurua-Olaizola O, et al. Glycosylation of extracellular vesicles: current knowledge, tools and clinical perspectives. Journal of Extracellular Vesicles. 2018; 7(1):1442985.

[12] Zhang JT, Qin H, Man Cheung FK, et al. Plasma extracellular vesicle microRNAs for pulmonary ground-glass nodules. Journal of extracellular vesicles. 2019; 8(1):1663666.

[13]Min L, Zhu S, Chen L, et al. Evaluation of circulating small extracellular vesicles derived miRNAs as biomarkers of early colon cancer: a comparison with plasma total miRNAs. Journal of extracellular vesicles. 2019; 8(1): 1643670.

[14]Witwer KW, Buzás EI, Bemis LT, et al. Standardization of sample collection, isolation and analysis methods in extracellular vesicle research. Journal of Extracellular Vesicles. 2013; 2(1):20360.

[15] Lötvall J, Hill AF, Hochberg F, et al. Minimal experimental requirements for definition of extracellular vesicles and their functions: a position statement from the International Society for Extracellular Vesicles. Journal of Extracellular Vesicles. 2014; 3:1.

[16] Islam MK, Syed P, Lehtinen L, et al. A nanoparticle-based approach for the detection of extracellular vesicles. Scientific reports. 2019; 9(1):1-9.

[17] Herrero C, de la Fuente A, Casas-Arozamena C, et al. Extracellular vesicles-based biomarkers represent a promising liquid biopsy in endometrial cancer. Cancers. 2019; 11(12): 2000.

[18] Nishida-Aoki N, Tominaga N, Kosaka N, et al. Altered biodistribution of deglycosylated extracellular vesicles through enhanced cellular uptake. Journal of extracellular vesicles. 2020; 9(1):1713527.

[19] Royo F, Cossío U, de Angulo AR, et al. Modification of the glycosylation of extracellular vesicles alters their biodistribution in mice. Nanoscale. 2019; 11(4): 1531-1537.

[20] Williams C, Pazos R, Royo F, et al. Assessing the role of surface glycans of extracellular vesicles on cellular uptake. Scientific reports. 2019; 9(1), 1-14.

[21] Berenguer J, Lagerweij T, Zhao XW, et al. Glycosylated extracellular vesicles released by glioblastoma cells are decorated by CCL18 allowing for cellular uptake via chemokine receptor CCR8. Journal of extracellular vesicles. 2018; 7(1): 1446660.

[22] Zen K, Zhang C Y. Circulating microRNAs: a novel class of biomarkers to diagnose and monitor human cancers[J]. Medicinal research reviews. 2012; 32(2): 326-348.

[23] Allegra A, Alonci A, Campo S, et al. Circulating microRNAs: new biomarkers in diagnosis, prognosis and treatment of cancer[J]. International journal of oncology. 2012; 41(6): 1897-1912.

[24] Gai C, Camussi F, Broccoletti R, et al. Salivary extracellular vesicle-associated miRNAs as potential biomarkers in oral squamous cell carcinoma. BMC cancer. 2018; 18(1):1-11.

[25] Guduric-Fuchs J, O'Connor A, Camp B, et al. Selective extracellular vesicle-mediated export of an overlapping set of microRNAs from multiple cell types. BMC genomics. 2012; 13(1):1-14.

[26] Tkach M, Théry C. Communication by extracellular vesicles: where we are and where we need to go. Cell. 2016; 164(6):1226-1232.

[27] Tian SC, Lim SK. Measurement of Precursor miRNA in Exosomes from Human ESC-Derived Mesenchymal Stem Cells. Methods in molecular biology (Clifton, N.J.). 2013; 1024(1024):69-86.

Figure legends

Figure 1. Workflow of the GlyExo-Capture technique.

LCA magnetic beads can specifically capture fucosylated extracellular vesicles from serum samples and cell supernatants. The whole process of preparing 96 samples only took 11 minutes. LCA: Lens culinaris lectin, HCC: hepatocellular carcinoma.

Figure 2. Characterization of fucosylated-EVs isolated by GlyExo-Capture technique.

(a,b) EVs isolated by GlyExo-Capture technique (GlyExo) and differential ultracentrifugation (UC) were analyzed under a transmission electron microscope (TEM; a) or Nanoparticle tracking analysis (NTA; b). The representative EVs were highlighted by arrows in (a). Scale bars, 100 nm. (c) GlyExo-EVs, UC-EVs, and whole cell lysate (WCL) were analyzed by western blotting using the indicated antibodies. (d) GlyExo-EVs and UC-EVs were analyzed by ExoView using the indicated antibodies. (e) The UC-EVs of HepG2 cells were incubated with LCA-immobilized beads or BSA-immobilized beads, and the bound fractions were subjected to quantitative analysis. The doses of EVs was quantified using Qubit Protein Assay and a Qubit3.0 fluorometer. EVs captured was calculated as bound fraction/UC-EVs loaded. (f) The UC-EVs of HepG2 or MIHA cells were incubated with LCA-immobilized beads and the bound fraction were subjected to quantitative analysis. Cell-based studies were performed independently at least three times with comparable results. Differences

were evaluated using two-tailed Student's t-tests. *P < 0.05, **P < 0.01, ***P < 0.001.

Figure 3. Cellular uptake of fucosylated-EVs.

(a,b) Flow cytometry analysis of DiD-labeled HF-EVs uptake by parental HepG2 cells. 20 μg DiD-labeled HF-EVs were added to HepG2 cells for the indicated time (a) or different amounts of DiD-labeled HF-EVs were added to HepG2 cells for 4 h (b). (c,d) Flow cytometry analysis of DiD-labeled HF-EVs or LF-EVs uptake by parental HepG2 cells in the presence or absence of PNGase F. Intracellular fluorescence intensity from DiD labeled EVs was quantitated as the percentage of positive cells (c) and the mean fluorescence intensity (MFI; d). (e,f) Flow cytometry analysis of DiD-labeled HF-EVs or LF-EVs uptake by HepG2, HCT-116, and Hela cells. Intracellular fluorescence intensity from DiD labeled EVs was quantitated as the percentage of positive cells (e) and the MFI (f). Cell-based studies were performed independently at least three times with comparable results. Differences were evaluated using two-tailed Student's t-tests. *P < 0.05, **P < 0.01, ***P < 0.001.

Figure 4. Verification of fucosylated-EVs miRNA expression in HCC.

(a) Linear discriminant analysis (LDA) based on the expression matrix of the 75 DEMs identified by Next-generation deep sequencing (NGS). Red dots are HCC patients, yellow dots are hepatitis and green dots are healthy controls. (b) A Venn diagram showed the common DEMs shared between TCGA dataset (blue circle) and fucosylated-EVs miRNA dataset (red circle). (c,d) The expressions of 13 randomly selected DEM by RT-qPCR or NGS. The expression of miRNA levels was normalized to

non-HCC groups (RT-qPCR). The expression pattern of miR-9-3p was shown in (c). The other 12 miRNAs were shown in (d). Differences were evaluated using the Mann-Whitney test. *P < 0.05, **P < 0.01, ***P < 0.001.

Figure 5. Identification of HCC-specific miRNA signatures in fucosylated-EVs.

(a) Paired scatter plot matrix of the 6 miRNA markers selected by the multivariate analysis of the original samples. (b,c) The expression of miR-432-5p and miR-215-5p (b) and miR-183-3p, miR-483-5p, miR-429, and miR-651-5p (c) by RT-qPCR in HCC and non-HCC controls. (d) Spearman correlation heatmap assay of the 4-miRNA including miR-183-3p, miR-483-5p, miR-429, and miR-651-5p. Differences were evaluated using the Mann-Whitney test. *P < 0.05, **P < 0.01, ***P < 0.001.

Figure 6. Diagnostic evaluation of the 4-miRNA panel in fucosylated-EVs.

(a) The prediction efficiencies using the widely-used models including Gradient Boost, AdaBoost, Random Forest, Bagging, Decision Tree, Gaussian NB, K Neighbors, SVC, and Logistic Regression based on the 4-miRNA panel in the training sample. (b) The prediction capabilities using AdaBoost model based on the 4-miRNA panel (Red line, AUC=0.86) or randomly selected 4 miRNAs in the testing sample(blue dots). (c-f) The expression of miR-182-3p (c), miR-429 (d), miR-651-5p (e),and miR-483-5p (f) using NGS data in the original sample and the validation sample. (g) Verification of the 4-miRNA panel as biomarkers of HCC in the validation sample (AUC=0.84). (h) The 4-miRNA panel improved the HCC diagnostic accuracy with AFP (AUC=0.92).

Differences were evaluated using the Mann-Whitney test. *P < 0.05, **P < 0.01, ***P < 0.001.

Supplemental Figure 1. Characterization of fucosylated-EVs, related to Figure 2.

A-B. Histograme of ExoView analysis of GlyExo-EVs (A) and UC-EVs(B) using the indicated antibodies. IgG was used as a negative control.DFA: Dilution Factor Adjusted.

Supplemental Figure 2. miRNA profiles of fucosylated-EVs in HCC,related to Figure 4.

A heatmap of the expression levels of the 75 DEMs across all the 115 samples in fucosylated-EVs derived miRNA dataset.

Supplemental Figure 3. miRNA pathway analysis of fucosylated-EVs in HCC,related to Figure 4.

Kyoto Encyclopedia of Genes and Genomes (KEGG) enrichment analysis (TOP 40 Terms ranked by p-value) of mRNAs targeted by the 75 DEMs identified in fucosylated-EVs derived miRNA dataset.

Supplemental Table 1. Key resources.

Supplemental Table 2. The primers used for RT–qPCR

Supplemental Table 3. The procedure for isolating EVs by GlyExo-Caputre technique.

Supplemental Table 4. The specificity and sensitivity of TOP 45 DEMs in identifying HCC patients in fucosylated-EVs derived miRNA dataset ranked by P-adj value.

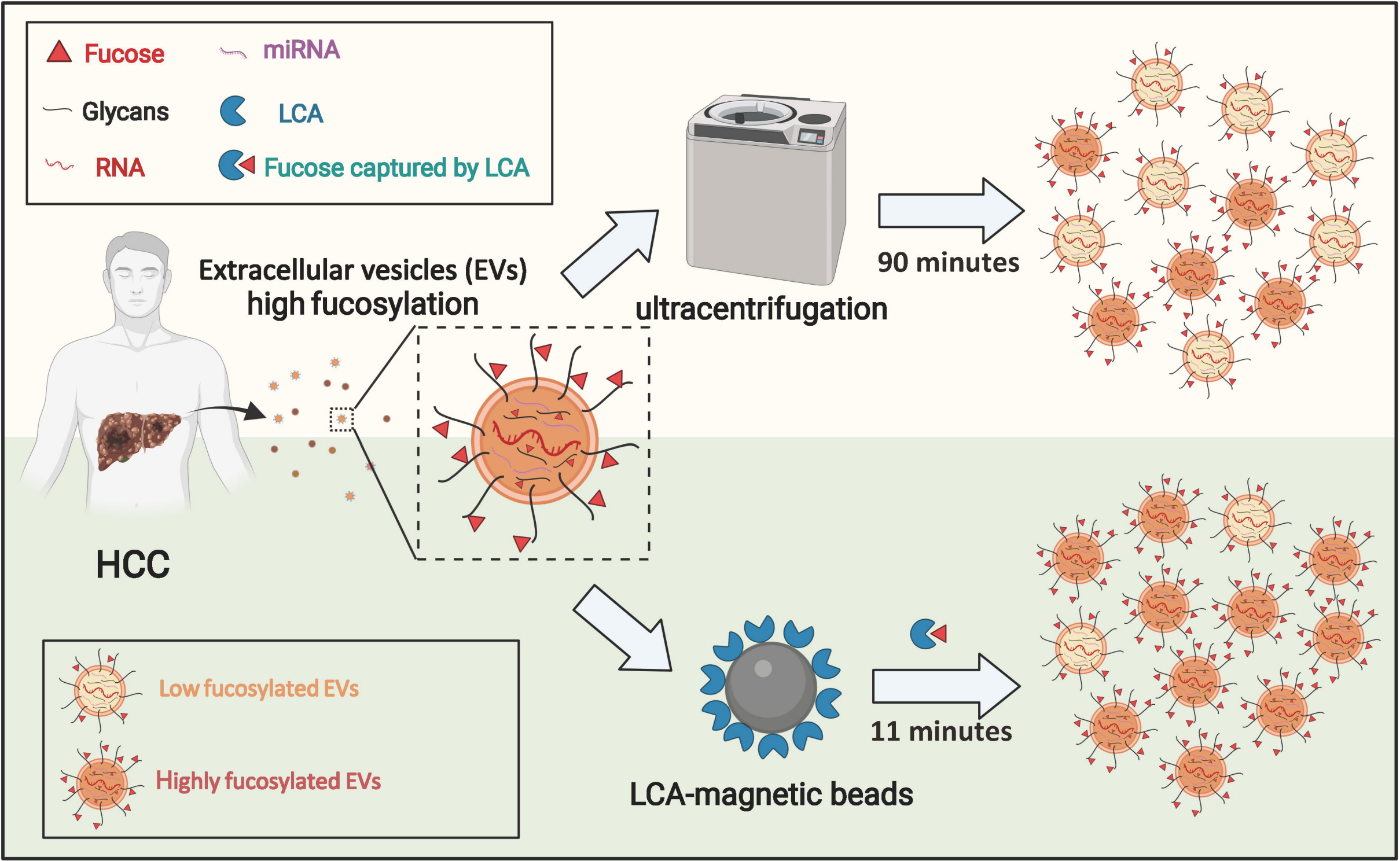
Fucose
miRNA
Glycans
LCA
RNA
Fucose captured by LCA
Extracellular vesicles (EVs)
high fucosylation
ultracentrifugation
90 minutes
HCC
Low fucosylated EVs
Highly fucosylated EVs
LCA-magnetic beads
11 minutes

Figure 2

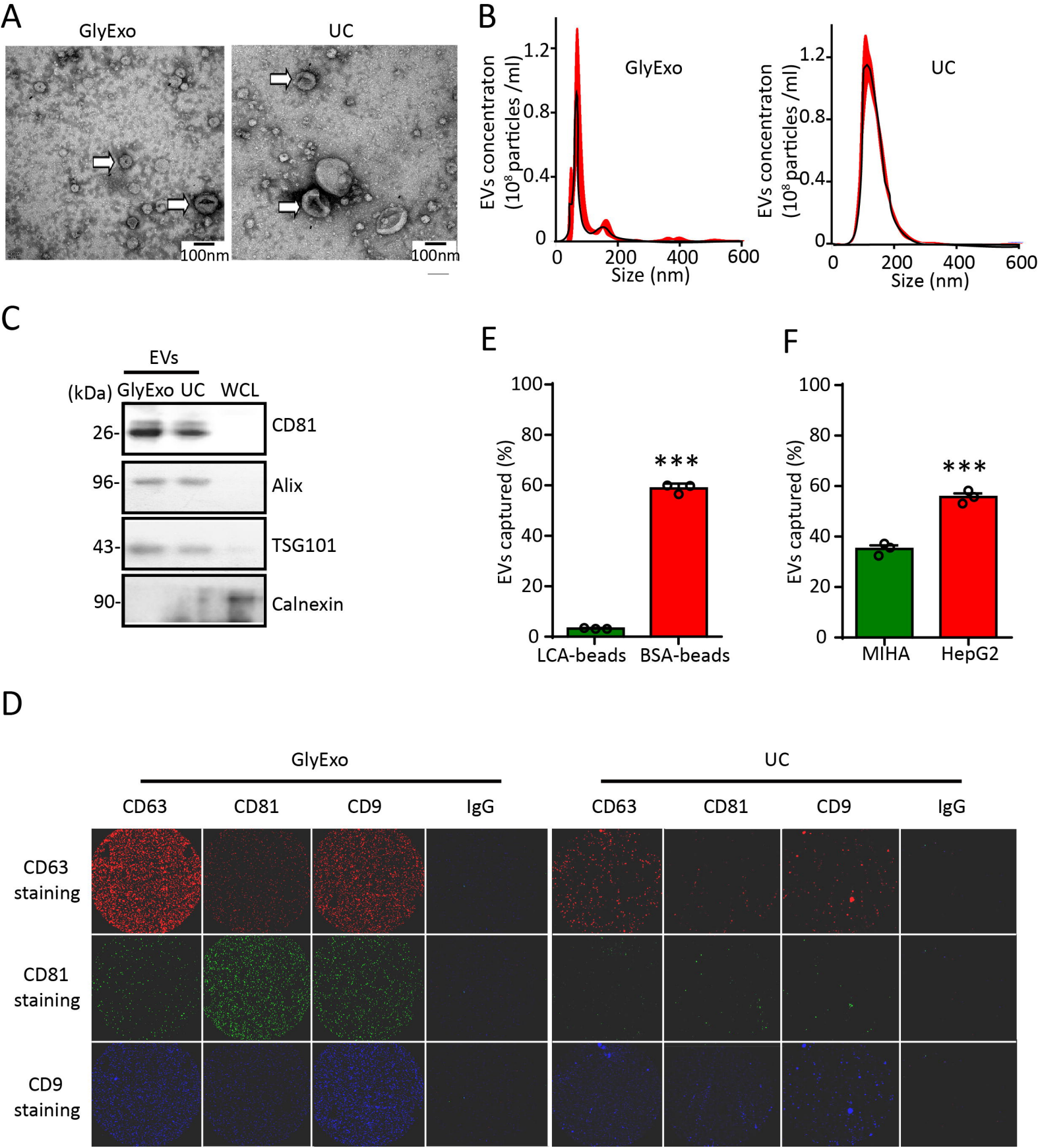
A
GlyExo
UC
100nm
100nm
B
GlyExo
UC
EVs concentraton (10^8 particles /ml)
1.2
0.8
0.4
0
0
200
400
600
Size (nm)
C
EVs
(kDa) GlyExo UC WCL
26-
96-
43-
90-
CD81
Alix
TSG101
Calnexin
E
EVs captured (%)
100
80
60
40
20
0
***
LCA-beads
BSA-beads
F
EVs captured (%)
100
80
60
40
20
0
***
MIHA
HepG2
D
GlyExo
UC
CD63
CD81
CD9
IgG
CD63 staining
CD81 staining
CD9 staining

Figure 3

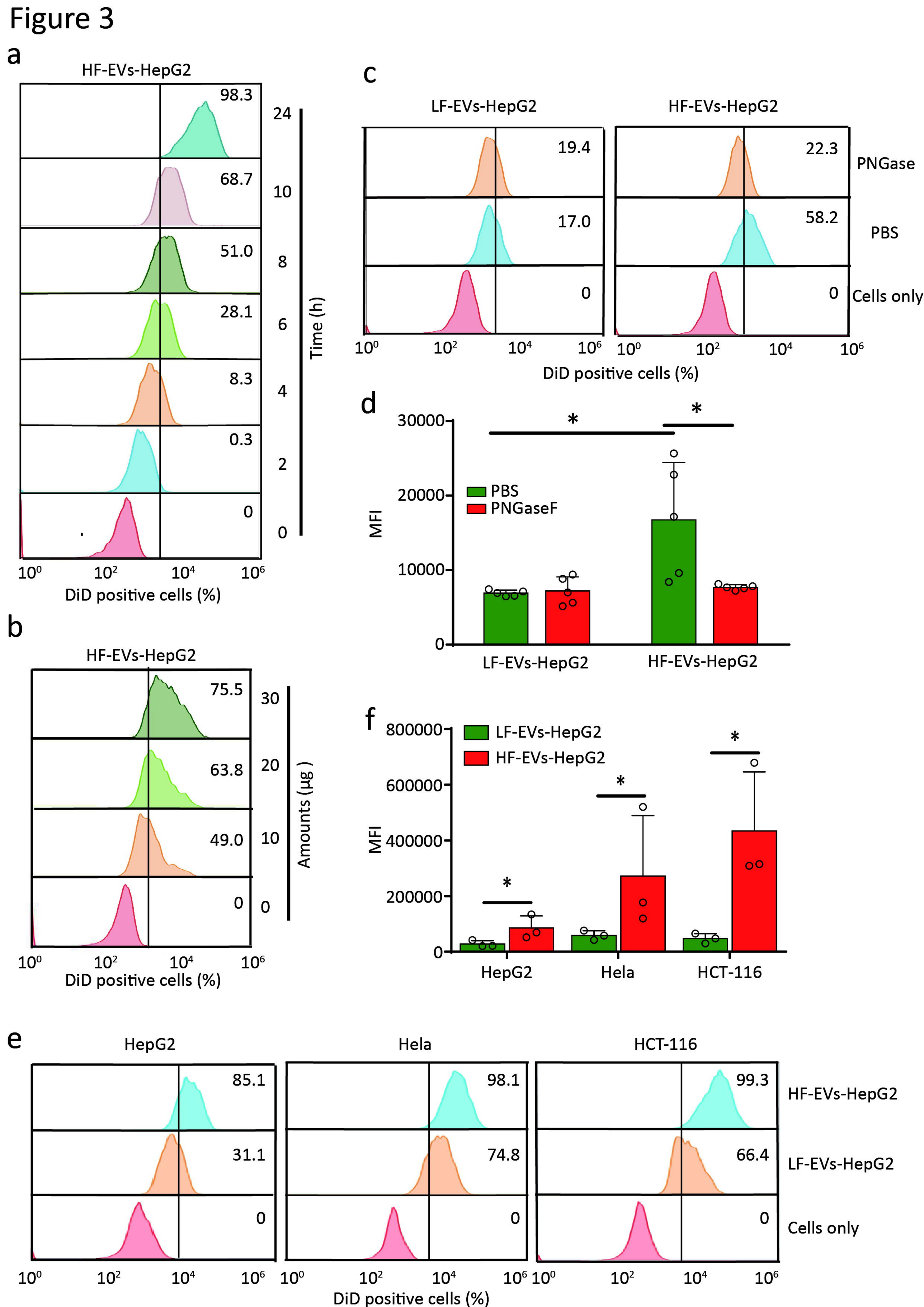
a
HF-EVs-HepG2
98.3
68.7
51.0
28.1
8.3
0.3
0
24
10
8
6
4
2
0
Time (h)
DiD positive cells (%)
b
HF-EVs-HepG2
75.5
63.8
49.0
0
30
20
10
0
Amounts (µg)
DiD positive cells (%)
c
LF-EVs-HepG2
HF-EVs-HepG2
19.4
17.0
0
22.3
58.2
0
PNGase
PBS
Cells only
DiD positive cells (%)
d
PBS
PNGaseF
MFI
LF-EVs-HepG2
HF-EVs-HepG2
e
HepG2
Hela
HCT-116
85.1
31.1
0
98.1
74.8
0
99.3
66.4
0
HF-EVs-HepG2
LF-EVs-HepG2
Cells only
DiD positive cells (%)
f
LF-EVs-HepG2
HF-EVs-HepG2
MFI
HepG2
Hela
HCT-116

Figure 4

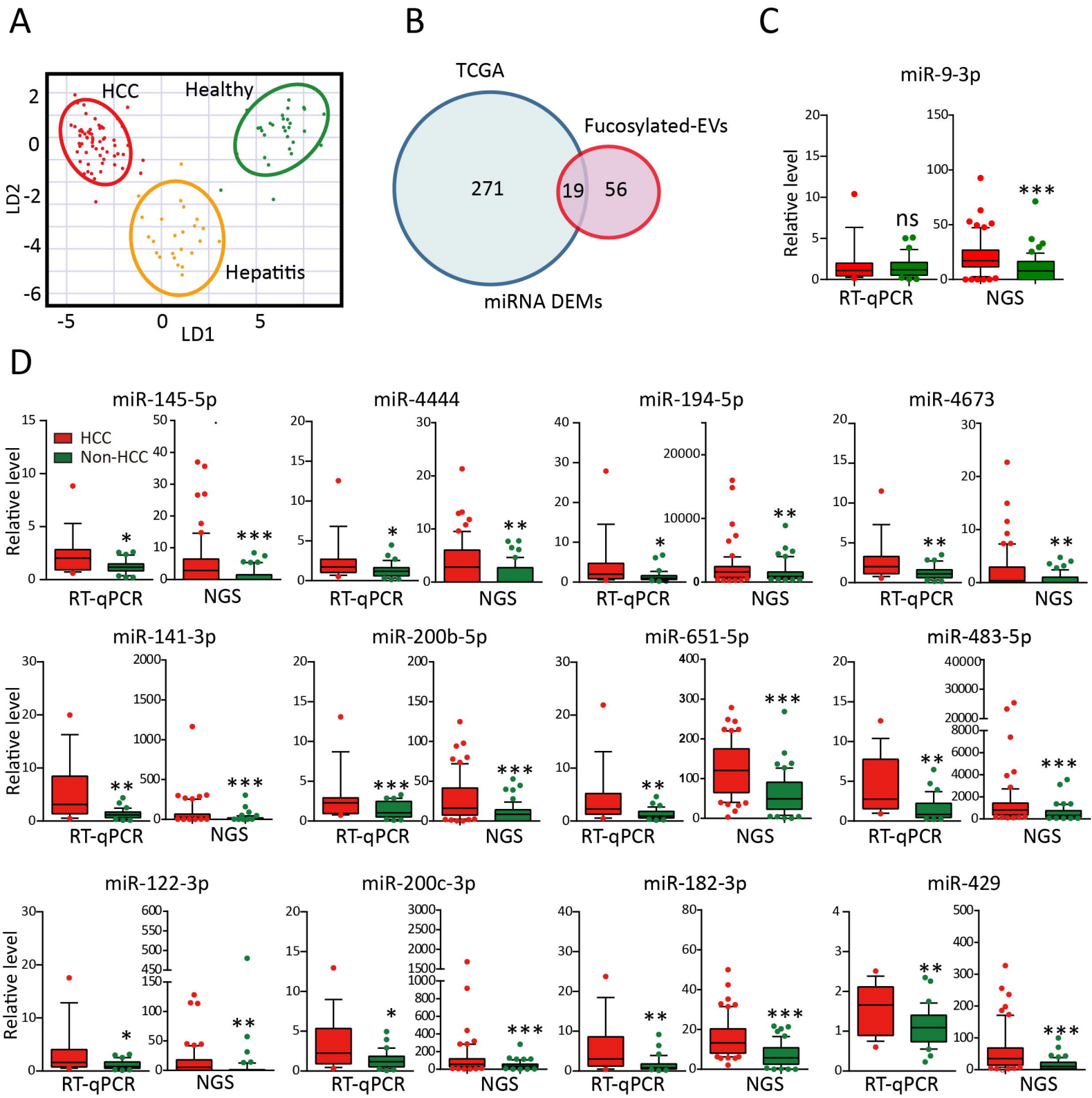
A
HCC
Healthy
Hepatitis
LD2
LD1
B
TCGA
Fucosylated-EVs
271
19
56
miRNA DEMs
C
miR-9-3p
Relative level
ns
***
RT-qPCR
NGS
D
HCC
Non-HCC
Relative level
miR-145-5p
miR-4444
miR-194-5p
miR-4673
miR-141-3p
miR-200b-5p
miR-651-5p
miR-483-5p
miR-122-3p
miR-200c-3p
miR-182-3p
miR-429
RT-qPCR
NGS

Figure 5

A

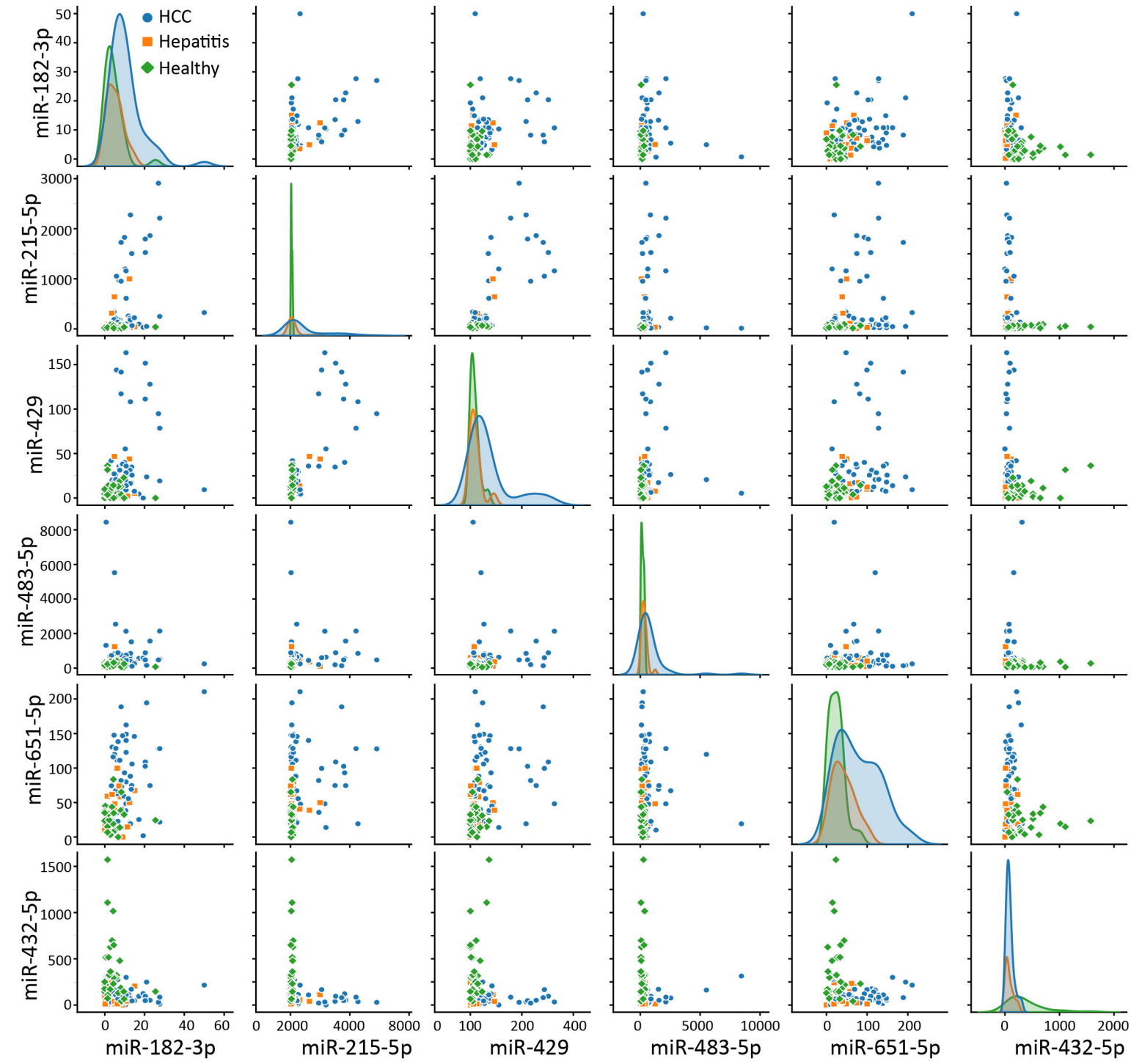

B

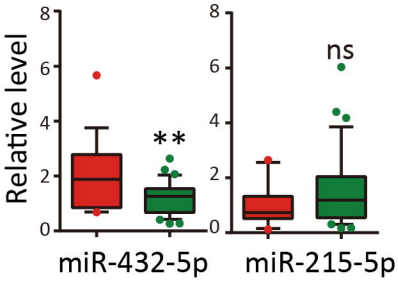

C

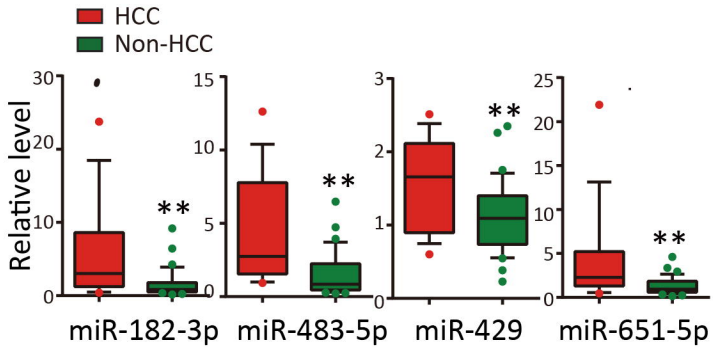

D

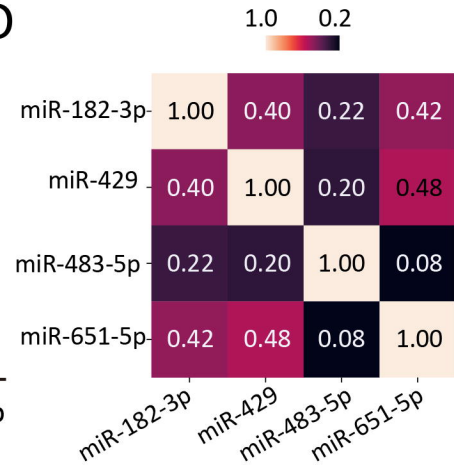

Figure 6

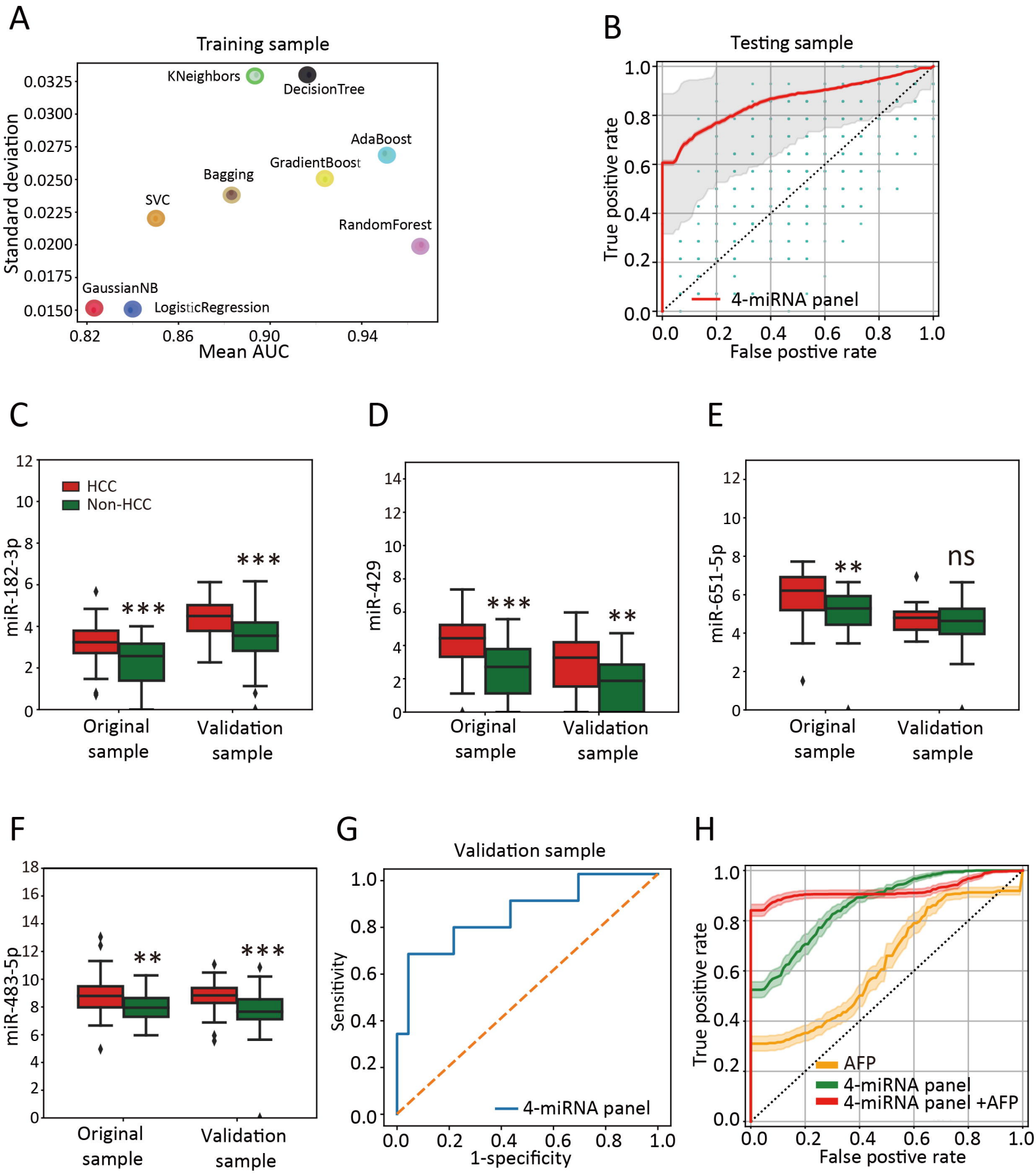
A
Training sample
KNeighbors
DecisionTree
AdaBoost
GradientBoost
Bagging
SVC
RandomForest
GaussianNB
LogisticRegression
Standard deviation
Mean AUC
B
Testing sample
True positive rate
False postive rate
4-miRNA panel
C
HCC
Non-HCC
miR-182-3p
Original sample
Validation sample
D
miR-429
E
miR-651-5p
ns
F
miR-483-5p
G
Validation sample
Sensitivity
1-specificity
4-miRNA panel
H
AFP
4-miRNA panel
4-miRNA panel +AFP